
# Boosting fine-grained activity sensing by embracing wireless multipath effects

Kai Niu
Peking University
Beijing, China
xjtunk@pku.edu.cn

Fusang Zhang
Peking University
Institute of Software, Chinese Academy of Sciences
Beijing, China
zhangfusang@otcaix.iscas.ac.cn

Jie Xiong
University of Massachusetts Amherst
Massachusetts, USA
jxiong@cs.umass.edu

Xiang Li
Peking University
Beijing, China
lixiang13@pku.edu.cn

Enze Yi
Peking University
Beijing, China
yienze_cs@pku.edu.cn

Daqing Zhang*
Peking University
Beijing, China
dqzhang@sei.pku.edu.cn

## ABSTRACT

With a big success in data communication, wireless signals are now exploited for fine-grained contactless activity sensing including human respiration monitoring, finger gesture recognition, subtle chin movement tracking when speaking, etc. Different from coarse-grained body and limb movements, these fine-grained movements are in the scale of millimetres and are thus difficult to be sensed. While good sensing performance can be achieved at one location, the performance degrades dramatically at a very nearby location. In this paper, by revealing the effect of static multipaths in sensing, we propose a novel method to add man-made "virtual" multipath to significantly improve the sensing performance. With carefully designed "virtual" multipath, we are able to boost the sensing performance at each location purely in software without any extra hardware.

We demonstrate the effectiveness of the proposed method on three fine-grained sensing applications with just one Wi-Fi transceiver-pair, each equipped with a single antenna. For respiration monitoring, we can remove the "blind spots" and achieve full coverage respiration sensing. For finger gesture recognition, our system can significantly increase the recognition accuracy from 33% to 81%. For chin movement tracking, we are able to count the number of spoken syllables in a sentence at an accuracy of 92.8%.

## CCS CONCEPTS

• **Human-centered computing** → **Ubiquitous computing**; **Ubiquitous and mobile computing systems and tools**;

## KEYWORDS

Wireless sensing; Fine-grained human activity; Multipath; Channel State Information

**ACM Reference Format:**
Kai Niu, Fusang Zhang, Jie Xiong, Xiang Li, Enze Yi, and Daqing Zhang. 2018. Boosting fine-grained activity sensing by embracing wireless multipath effects. In *The 14th International Conference on emerging Networking EXperiments and Technologies (CoNEXT '18), December 4–7, 2018, Heraklion, Greece.* ACM, New York, NY, USA, 13 pages. https://doi.org/10.1145/3281411.3281425

*Corresponding author


*CoNEXT '18, December 4–7, 2018, Heraklion, Greece*

ACM ISBN 978-1-4503-6080-7/18/12…$15.00
https://doi.org/10.1145/3281411.3281425

## 1 INTRODUCTION

Wireless technologies have achieved a great success in data communication in the last two decades. In recent years, the research community has explored the opportunities of applying wireless signals for sensing human being and our surrounding environment. With pervasive Radio Frequency (RF) signals such as Wi-Fi and RFID in our ambient environment, wireless sensing is able to enable a large variety of new applications, ranging from coarse-grained indoor localization [5, 39], trajectory tracking [15, 21, 25, 35, 36], gait/gesture recognition [10, 12, 19, 23, 27, 33] to fine-grained vital sign monitoring [6, 9, 16, 17, 29, 42–44], keystroke detection [7, 13] and lip reading [28]. Compared to coarse-grained activities, subtle fine-grained activities only cause very small signal variations which are non-trivial to be captured. More severely, the sensing performance is unstable and highly dependent on the target's relative positions with respect to the transceivers. The "blind spots" issue was reported in human respiration sensing research using Wi-Fi signals [29, 41]. While good respiration sensing performance can be achieved at some locations, the performance at other locations (blind spots) can be quite poor. The same issue happens to other fine-grained sensing applications such as small-scale finger gesture recognition and chin movement tracking when speaking. A small one centimetre change in location can lead to a significant degradation in the performance of finger gesture recognition. This performance instability issue restricts the practical adoption of these sensing systems in real life.

The existing works assert the unstable sensing performance is mainly due to multipath and quite a lot of methods are proposed

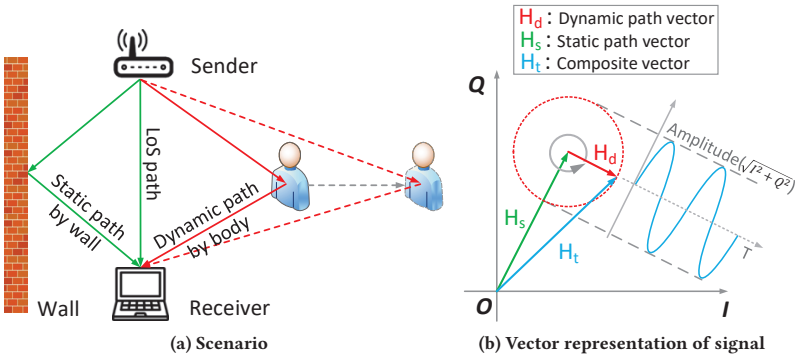


**Figure 1: Signal variation caused by human movement**

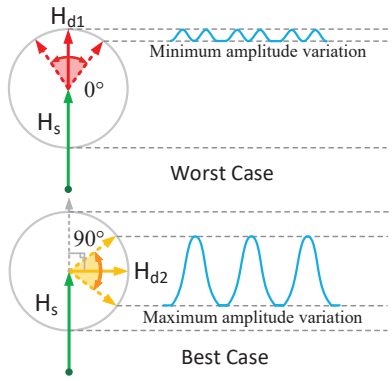


**Figure 2: Good position vs. bad position**

to either remove the multipath [28, 30, 32, 40] or avoid the interference of multipath [38] by selecting subcarriers or channels not affected by multipath. On the other hand, separating and removing multipath are quite challenging. Even with the help of advanced signal processing techniques and dedicated hardware such as phased antenna arrays, the performance of multipath removal is still not satisfactory [28], requiring further research in this area.

In this work, we study the wireless signal propagation theory to explain the reason why unstable sensing performance occurs for fine-grained activity sensing and propose a novel method to address the issue. Instead of trying to separate and remove the multipath which is challenging, we create one extra "virtual" multipath in software and utilize the created multipath to help improve the wireless sensing performance.

More specifically, we observe that at different locations, the same subtle movement can induce very different signal variations, causing unstable wireless sensing performance. When the movement-induced signal variation becomes too small, the movement can hardly be detected and the sensing performance becomes poor. The fundamental reason behind this issue is that the movement-induced dynamic reflection signal vector has varying phase differences with respect to the composite static signal vector at different locations and this phase difference actually determines the amplitude of the captured signal variation and accordingly the sensing capability. By changing the target's physical position, it is possible to vary this phase difference and find those physical positions at where good sensing performance can be achieved. However, changing the target's physical position is not only inconvenient but also intrusive. In practice, it is also very difficult to change the target's position by a precise small amount say 2cm. Inspired by the feasibility of creating a real multipath via placing a metal plate besides the transceiver to improve the sensing performance, we propose to inject "virtual" multipath in software to enlarge the signal variation caused by the target movement without requiring to change the target's physical position nor to place one physical reflector. With carefully designed "virtual" multipath, we can tune the phase difference to the expected value to maximize the sensing performance purely in software.

Assuming there is only one moving object in a static environment as shown in Figure 1a, we could group the signal paths reaching the receiver into two categories: dynamic path and static paths. The dynamic path is the signal path induced by the moving target while the static paths are composed of the direct path and reflected paths from the walls and static objects in the environment. If we represent the signals of dynamic and static paths as space vectors, the dynamic path vector induced by the target's movement rotates with respect to the composite static path vector as shown in Figure 1b, inducing sinusoidal-like signal variation. In essence, the phase difference between the dynamic vector and static vector is the key factor which determines the sensing performance. As shown in Figure 2, for the same movement, the signal variation is much larger when the phase difference is 90 degrees than when the phase is 0 degree. By adding a "virtual" multipath, we are able to control the phase difference between the dynamic path and the composite static path, maximizing the signal variation and improving the sensing performance.

The main contributions of this work are summarized as follows:

(1) This work addresses one important issue of fine-grained wireless sensing: the sensing performance is unstable and there are always "blind spots" at where the sensing performance is extremely poor. From the vector representation perspective, we explain the reason theoretically and verify it with experiments.
(2) We investigate the multipath effects on sensing in theory and propose to add "virtual" multipath in software to boost the sensing performance at "blind spots". We believe the principle can be extended to improve sensing performance with other technologies such as RFID and sound.
(3) We demonstrate the effectiveness of our method by applying it on three Wi-Fi based fine-grained sensing applications: (i) respiration detection; (ii) finger gesture recognition and (iii) chin movement tracking when speaking. Extensive experiments show that our method can significantly improve the sensing performance. We envision it as a general method to be applied to benefit a large range of wireless sensing applications.

## 2 PRELIMINARY

In this section, we first introduce the basics of wireless sensing. Then we model the fine-grained human activities and present the insight to improve sensing performance.

**Table 1: The movement displacement of fine-grained activities**

| Scenario | Movement displacement | Path length change | Phase change |
|---|---|---|---|
| Normal breathing (Anteroposterior dimension) | $4.2 \sim 5.4mm$ | $\leq 1.08cm$ | $\leq 68^{\circ}(\leq 0.5\pi)$ |
| Deep breathing (Anteroposterior dimension) | $6 \sim 11mm$ | $\leq 2.2cm$ | $\leq 140^{\circ}(\leq \pi)$ |
| Chin displacement (Distance to Los $\leq 20cm$) | $5 \sim 20mm$ | $\leq 1.42cm$ | $\leq 89^{\circ}(\leq 0.5\pi)$ |
| Finger displacement (Distance to Los $\leq 20cm$) | $15 \sim 40mm$ | $\leq 2.71cm$ | $\leq 170^{\circ}(\leq \pi)$ |

## 2.1 Modeling wireless sensing

Wireless signals arrive at the receiver through multiple paths from the receiver. Channel State Information (CSI) is used to quantify the wireless channel between the transmitter-receiver (Tx-Rx) pair. Each path has its own Channel State Information (CSI). In essence, CSI characterizes the *Channel Frequency Response* (CFR) between an antenna pair which is known as a link. For carrier frequency $f$ of each link, the CSI ($H(f,t)$) at time $t$ has the relationship $Y(f,t) = H(f,t) \times X(f,t)$, where $X(f,t)$ and $Y(f,t)$ are the frequency domain representations of the transmitted and received signals, respectively [34].

If an RF signal arrives at the receiver through $N$ different paths, then the total CSI is the linear superposition of all paths' CSIs, which can be denoted as

$$\begin{aligned} H(f,t) &= \sum_{k=1}^{N} H_k(f,t) \\ &= \sum_{k=1}^{N} |H_k(f,t)| e^{-j \cdot 2\pi d_k/\lambda} \end{aligned} \tag{1}$$

where $H_k(f,t)$ is the Channel State Information (CSI) of the $k^{th}$ path, $|H_k(f,t)|$ is amplitude of $H_k(f,t)$, $d_k$ is the length of the $k$th path, and $\lambda$ is the wavelength for carrier frequency $f$.

The phase of a Wi-Fi signal rotates when the signal propagates in the air. Consider a scenario in Figure 1a, where the Wi-Fi signal is also reflected by wall and human body besides the Line-of-Sight (LoS) path. The LoS path and the path from the static wall are static paths. The CSI of a static path is a constant in a short period of time. On the other hand, the path reflected from a moving target is called a dynamic path and the CSI changes with the movement. In the complex plane in Figure 1b, $H_s$ represents the static path component which contains the LoS path and the reflected path from the wall. $H_d$ represents the dynamic path. $H_t$ is the resultant signal received at the receiver and is the linear superposition of $H_s$ and $H_d$. When human target moves, the dynamic path changes accordingly. Within a short period of time, the signal amplitude of dynamic vector can be considered as a constant but the phase changes dramatically. The phase change causes the dynamic vector $H_d$ to rotate with respect to the static vector $H_s$, as shown in Figure 1b. Thus, the resultant signal $H_t$ also changes with the dynamic path signal. The amplitude of the resultant signal $H_t$ changes like a sinusoidal curve, denoted as

$$|H_t|^2 = |H_s|^2 + |H_d|^2 + 2|H_s||H_d|\cos(\theta_s - \theta_d) \tag{2}$$

When the length of the dynamic path gets changed by $\lambda$, its phase rotates a full circle ($2\pi$), which means $H_d$ rotates 360 degrees.

## 2.2 Sensing fine-grained human activities

We first present the model of subtle movements caused by fine-grained activities. We analyze three typical activities, i.e., human respiration, small-scale finger movement, and chin movement when speaking, as shown in Figure 3. Human respiration involves respiratory cycles of inhalation and exhalation with expansion and contraction of lungs. Hence, the human chest can be modeled as a varying-size semi-cylinder, where the outer cylinder surface corresponds to the chest positions during the process of respiration [29]. The outer cylinder surface is a moving reflector for the RF signal. When we speak, our chin slightly moves and becomes a moving reflector, inducing RF signal variations. Similarly, for finger movement, the finger moves slightly for various finger gestures, causing RF signal variations.

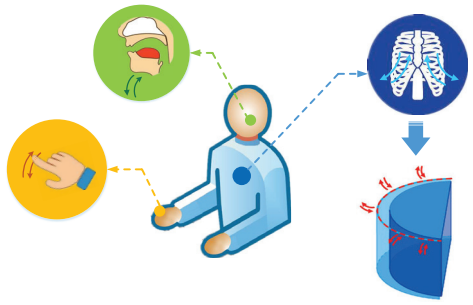

**Figure 3: Fine-grained human activities: finger gesture,chin movement when speaking, respiration**

In order to sense these fine-grained activities, it is necessary to understand how the received RF signal varies with the signal propagation length change due to the subtle movement. Table 1 presents the amount of movement displacement, path length change and phase change at a carrier frequency of 5.24GHz for the three fine-grained activities. From Table 1, we can see that the path length change induced by fine-grained activity movement is less than $\lambda/2$ ($2.86cm$). Thus the signal variation is a fragment of the sinusoidal waveform. It is obvious that the larger the signal variation induced, the easier the movement can be sensed (detected). However, the same amount of movement induces very different signal variations as shown in Figure 2. We reveal that the phase difference between the dynamic vector and static vector is the key to determine the signal variations (Section 3).

Intuitively, there are two ways we can change the phase difference to enlarge the signal variation. One way is to adjust the phase of the dynamic vector by changing the target's physical location. This method requires the target to change the position, which is

intrusive. The other way is to adjust the phase of the static vector, which does not require participation of the target. Initially, we change the phase of the static vector by introducing a real multipath created with a metal plate placed besides the transceiver. However, adjusting the position and orientation of the metal plate for the required multipath is neither convenient nor practical in real life. Thus, we propose to add a "virtual" multipath to change the phase of the static vector. The "virtual" multipath serves exactly the same role as a real static multipath and at the same time, eliminates the need of an extra metal plate as a reflector.

In the next section, we will quantify the sensing capability with signal variation and introduce our method to leverage multipath to improve the sensing performance.

## 3 ENHANCING FINE-GRAINED ACTIVITY SENSING WITH MULTIPATH

In this section, we first propose metrics to characterize the sensing capability and derive the factors affecting the sensing capability. With the detailed quantitative analysis, we clearly explain how to control the multipath to improve the sensing capability at each position. At last, we describe how to apply the proposed method to improve the performance of the sensing applications.

### 3.1 The sensing capability analysis for fine-grained activities

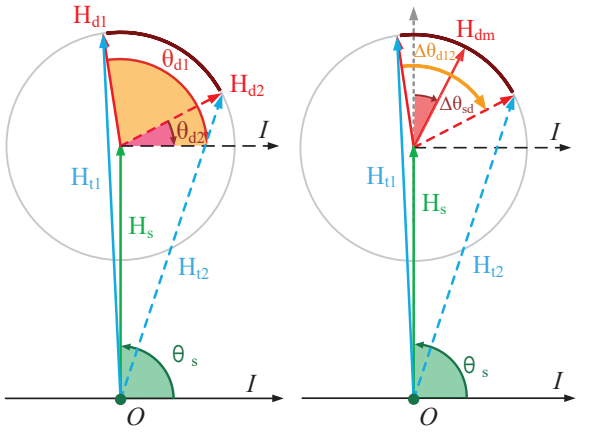


(a) Amplitude difference (b) Representation of $\Delta\theta_{sd}$ and $\Delta\theta_{d12}$

**Figure 4: Vector representation for amplitude difference and affecting factors**

The sensing capability is quantitatively related to the signal amplitude variation caused by the movement. The amplitude difference can be calculated as

$$\Delta|H| = |H_{t2}| - |H_{t1}| = \frac{|H_{t2}|^2 - |H_{t1}|^2}{|H_{t1}| + |H_{t2}|} \tag{3}$$

Placing Equation 2 into Equation 3, we obtain

$$\begin{aligned}\Delta|H| &= \frac{2|H_s||H_d|\cos(\theta_s - \theta_{d2}) - 2|H_s||H_d|\cos(\theta_s - \theta_{d1})}{|H_{t1}| + |H_{t2}|} \\ &= \frac{4|H_s||H_d|\sin(\theta_s - \frac{\theta_{d2}+\theta_{d1}}{2})\sin\frac{\theta_{d2}-\theta_{d1}}{2}}{|H_{t1}| + |H_{t2}|}\end{aligned} \tag{4}$$

where $\theta_s$,$\theta_{d1}$,$\theta_{d2}$ are the phases of signal vector $H_s$, $H_{d1}$, $H_{d2}$ respectively. $|H_{t1}|$ and $|H_{t2}|$ are the amplitudes of the composite vector $H_{t1}$, $H_{t2}$, as shown in Figure 4a. Note that for a small-scale movement, the amplitude of the dynamic vector can be considered as a constant[1] so $|H_{d1}| = |H_{d2}| = |H_d|$. To simplify Equation 4, we define the phase difference between the dynamic path and static path as $\Delta\theta_{sd}$

$$\Delta\theta_{sd} = \theta_s - \frac{\theta_{d2} + \theta_{d1}}{2}. \tag{5}$$

We define the phase change of the dynamic vector as $\Delta\theta_{d12}$

$$\Delta\theta_{d12} = \theta_{d2} - \theta_{d1} \tag{6}$$

$\Delta\theta_{sd}$ and $\Delta\theta_{d12}$ are both shown in Figure 4b. With the two defined new parameters, the amplitude difference can now be simplified as

$$\Delta|H| = \frac{4|H_s||H_d|\sin\Delta\theta_{sd}\sin\frac{\Delta\theta_{d12}}{2}}{|H_{t1}| + |H_{t2}|} \tag{7}$$

As the dynamic vector represents the much weaker reflected signal, $|H_d|$ is much smaller than $|H_s|$ ($|H_s| \gg |H_d|$). Thus, $|H_{t1}| \approx |H_s|$ and $|H_{t2}| \approx |H_s|$. So Equation 7 can be simplified as

$$\Delta|H| = 2|H_d|\sin\Delta\theta_{sd}\sin\frac{\Delta\theta_{d12}}{2} \tag{8}$$

So the sensing capability can now be defined as

$$\eta = ||H_d|\sin\Delta\theta_{sd}\sin\frac{\Delta\theta_{d12}}{2}| \tag{9}$$

From Equation 9, we can see that the sensing capability is determined by three factors: (i) the magnitude of the dynamic vector $|H_d|$; (ii) the phase difference between the static vector and dynamic vector $\Delta\theta_{sd}$ and (iii) the phase change of the dynamic vector due to subtle movement $\Delta\theta_{d12}$. We discuss the three factors and corresponding physical interpretations below.

- $|H_d|$ is the magnitude of the dynamic vector. $|H_d|$ is generally much smaller than $|H_s|$, because it is a reflected signal. $|H_d|$ becomes even smaller with a larger path length as the reflected signal needs to propagate longer distance in the air. That is to say, when the target is far away from the Tx-Rx pair, the sensing capability is poor. For a specific sensing position, the amplitude $|H_d|$ remains roughly the same during the process of these subtle movements such as human respiration and chin movement.
- $\Delta\theta_{sd}$ is the phase difference between the static vector $H_s$ and the dynamic vector $H_{dm}$. Since the dynamic vector has a starting point and an ending point, we employ $H_{dm}$ to represent the average of the two. The static vector $H_s$ remains unchanged. When the length of the reflection path changes by one wavelength[2], the dynamic vector $H_d$ rotates

[1] The signal amplitude is related to the path length. A 2-3cm path length change is negligible compared to the meter-level path length and thus signal amplitude can be assumed as a constant.

[2] $\lambda$ = 5.73cm for a carrier frequency of 5.24GHz

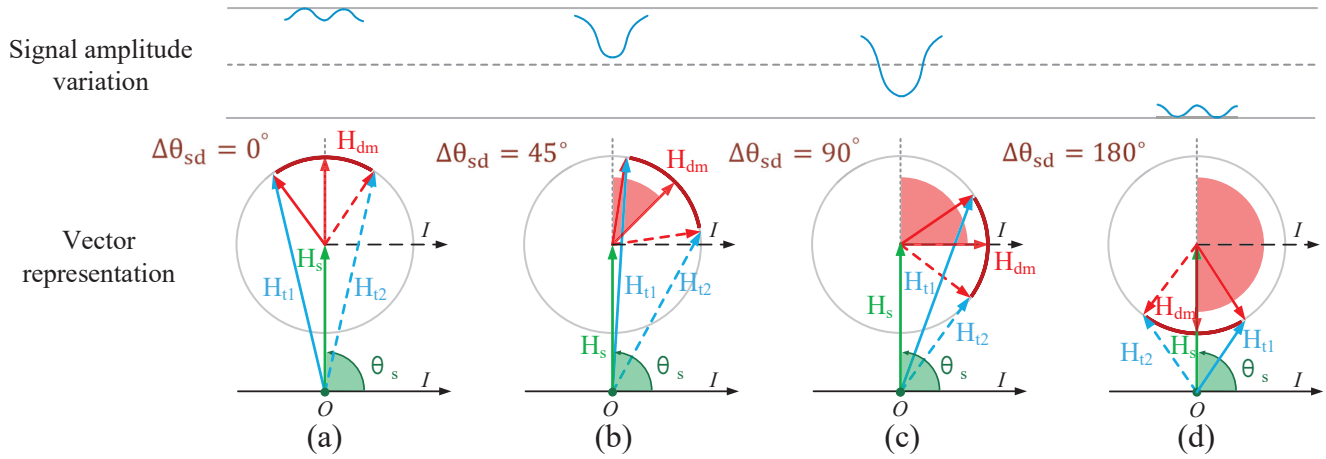


**Figure 5: The relation between detectability of subtle movements and sensing capability phase**

a full circle (360°). So a few centimetres of change in target's position results in a non-negligible change in $\Delta\theta_{sd}$, affecting the sensing capability. The value of $\sin\Delta\theta_{sd}$ is between 0 and 1. When the dynamic vector and the static vector are at the same direction, $\sin\Delta\theta_{sd}$ is 0. This induces a minimum signal variation which is easily merged by noises, leading to undetectability of the movement. When the dynamic vector is perpendicular to the static vector, $\Delta\theta_{sd}$ is 90° and the maximum signal variation is obtained with a high sensing capability. This phase difference is thus termed as *sensing capability phase*.

- $\Delta\theta_{d12}$ is the phase change of the dynamic vector during the process of a subtle movement. It is determined by the path length change of the dynamic path and is related to the displacement of the subtle movement. For instance, $\Delta\theta_{d12}$ is determined by the breath depth for respiration and the amount of chin movement when speaking.

Among the three factors, $\Delta\theta_{sd}$ is the key determining factor for the sensing performance. We study the effect of $\Delta\theta_{sd}$ on the sensing performance with a same subtle movement. Figure 5 shows the signal amplitude variation with four typical sensing capability phases. We can see that, when $\Delta\theta_{sd} = 0°$, the movement causes a minimum amount of signal variation. This small variation may easily becomes undetectable in a real-life noisy environment. This is the situation when "blind spots" occur. If the target moves slightly to a second location and now $\Delta\theta_{sd} = 45°$, we can see that the same amount of movement induces a larger signal variation and the whole movement-caused phase change is in a monotonic interval. If the target moves further, the dynamic vector continues to rotate right. Let's consider the scenario when the dynamic vector $H_{dm}$ is perpendicular to the static vector $H_s$ as shown in Figure 5c, we obtain the largest variation and this position has the best sensing performance. If the target moves further to the position when the dynamic vector $H_{dm}$ becomes parallel to the static vector as shown in Figure 5d, $\Delta\theta_{sd} = 180°$ which is again bad for sensing.

## 3.2 Improving sensing performance with multipath

From the previous section, we know the phase difference ($\Delta\theta_{sd}$) between the dynamic and static vector is the key factor affecting the sensing performance. We propose to leverage multipath, which is commonly considered harmful in existing sensing literature, to change the phase of the static vector.

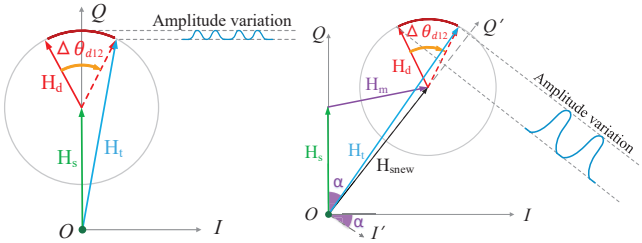


**Figure 6: The effect of adding multipath**

As shown in Figure 6, when a new static multipath is introduced, the original static vector and the new multipath vector together form a new static vector. The dynamic vector is not changed but now rotates around the new static vector. From the perspective of vector transformation, adding such a multipath actually transforms the original $IQ$ vector space to the new $I'Q'$ vector space as shown in Figure 6(b). After introducing a static virtual multipath, the static vector would be rotated from $H_s$ to $H_{snew}$, making the variation of the dynamic vector more distinguishable. With this multipath added in, we can now tune the sensing capability phase to turn a bad position into a good position for sensing. That is to say, we can utilize the multipath to control the sensing capability at each location. The sensing capability after the multipath is added changes to

$$\eta = ||H_d| \sin(\Delta\theta_{sd} - \alpha) \sin\frac{\Delta\theta_{d12}}{2}| \quad (10)$$

The problem now is how we can change the phase of the static vector to the right value to improve sensing performance. Note

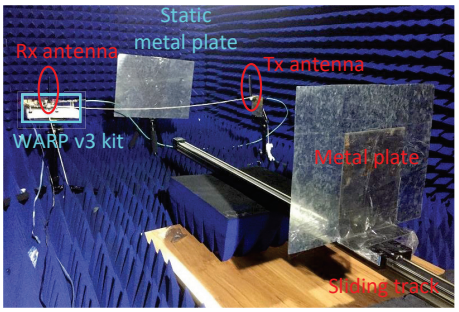


**Figure 7: Introduce multipath by metal plate**

that introducing new static objects into the environment can create extra multipaths, which will change the static vector. To verify this, we move a metal plate 5*mm* forward and then 5*mm* backward with the help of a sliding track to mimic the fine-grained activity in an anechoic chamber as shown in Figure 7. We then place the metal plate at a position with bad sensing performance. As shown in Figure 8a, the signal variation is very small and thus it is difficult to identify the 10 repetitive movements. Then without changing the position of the first metal plate, we create a new real multipath by placing a static metal plate besides the transceiver. After we carefully adjust the metal plate, the signal variation becomes clear enough to identify the 10 repetitive small movements, as shown in Figure 8b. This benchmark experiment demonstrates the feasibility of introducing extra multipath with an object to enhance the sensing performance.

However, there are a few issues in creating multipath with physical objects. First of all, due to the large surface area of the object, it is non-trivial to precisely control the created reflection (multipath) generated. Furthermore, when the transceiver's location gets changed, the object's physical location needs to be adjusted carefully and this process requires human intervention which is time-consuming and inconvenient.

To bypass the problems above, we propose a software based approach to create virtual multipath to control the sensing capability. As shown in Figure 8c, a virtual multipath can serve the same role as a real static multipath. The whole process of virtual multipath addition contains the following three steps:

**Step 1: Search Scheme for Phase Shift.** As shown in Figure 6, a new multipath changes the phase of the static vector by $\alpha$. And the phase shift can change the detectability of fine-grained activities. However, we have no idea of the original sensing capability phase $\Delta\theta_{sd}$ from the original signal. Therefore, we propose a searching scheme to transverse all possible phase shifts. Let phase shift $\alpha$ vary from 0 to $2\pi$ with a fixed step size, e.g., $\frac{\pi}{180}$, then the sensing capability phase $\Delta\theta_{sd} + \alpha$ also varies between 0 to $2\pi$, even though the original sensing capability phase $\Delta\theta_{sd}$ is unknown. With a brute-force trial of all possible phase shifts, the optimal phase shift which maximizes the sensing capability is one of them.

**Step 2: Calculating Multipath Vector.** Given the phase shift $\alpha$ varies from 0 to $2\pi$ in Step 1, we explain how to calculate the corresponding multipath vector. To understand the vector representation quantitatively, we construct a *triangle* to show the effect of added multipath on the phase shift in Figure 9a. $H_s$, $H_m$, and $H_{snew}$

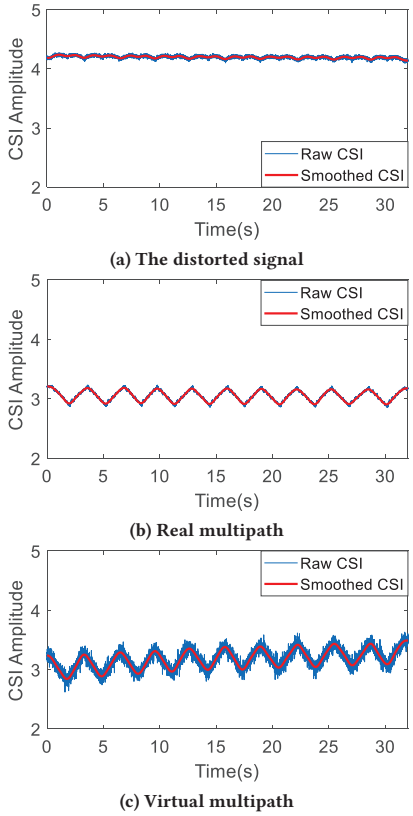


**(a) The distorted signal**

**(b) Real multipath**

**(c) Virtual multipath**

**Figure 8: The enhanced sensing signals by adding real multipath and virtual multipath**

are the static vector, multipath vector and new static vector, respectively. To determine the multipath vector $H_m$, firstly, we estimate the static vector by averaging a period of the composite vector $H_t$. This is an approximate estimation to obtain the static vector, which introduces a slight deviation from the original sensing capability phase. Our search scheme inherently overcomes this estimation deviation, because it traverses all possible phases of shift to add the multipath vector.

As shown in Figure 9b, for two different lengths of $|H_{snew1}|$ and $|H_{snew2}|$, two different multipaths $|H_{m1}|$ and $|H_{m2}|$ will be obtained. However, the same phase shift $\alpha$ is achieved to ensure the same amount of improvement in sensing performance. To simplify the problem, the amplitude of $H_{snew}$ is set equal to $|H_s|$ and this value does not affect the phase shift $\alpha$.

As shown in Figure 9a, for the *triangle* constructed above, the static vector $H_s$, the amplitude of $H_{snew}$ and the phase shift $\alpha$ are known now. Thus we can calculate the multipath vector $H_m$, including both the amplitude and phase. According to the law of cosines, the amplitude of $H_m$ is calculated as

$$|H_m| = \sqrt{(|H_s|^2) + |H_{snew}|^2 - 2|H_s||H_{snew}|\cos(\alpha)} \quad (11)$$

To obtain the phase of $H_m$, we employ the theorem $\frac{|Hm|}{\sin\alpha} = \frac{|H_{snew}|}{\sin\beta}$. The phase between the static vector and multipath vector $\beta$ is calculated as $\arcsin\frac{\sin\alpha|H_{snew}|}{|H_m|}$. Thus the phase of the added multipath

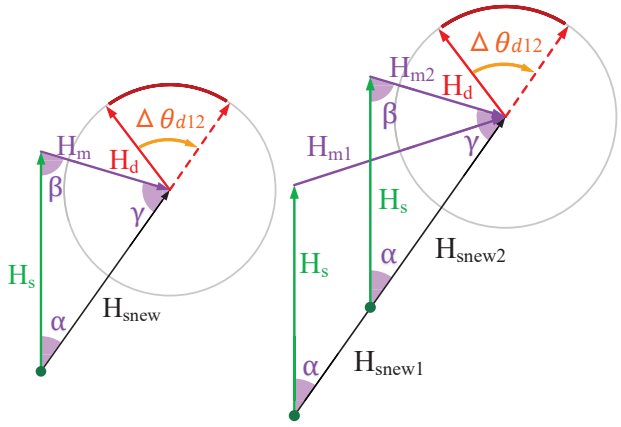


(a) Triangle construction (b) Different ways to add multipath

**Figure 9: Qualify the effect of multipath by constructing a triangle**

vector is calculated as

$$\theta_m = \theta_s + \beta - \pi \tag{12}$$

For a given phase shift $\alpha$, the multipath vector is calculated as $H_m = |H_m|e^{-j\theta_m}$.

**Step 3: Adding Multipath in Software.** After obtaining the multipath in vector form $H_m = |H_m|e^{-j\theta_m}$, we can create the required multipath in software and add it on-to the original signal. For a period of original signal with $N$ CSI samples $S_o = (CSI_1, CSI_2, ..., CSI_N)$, the new signal after adding multipath is $S(H_m) = (CSI_1 + H_m, CSI_2 + H_m, ..., CSI_N + H_m)$.

From the search scheme in Step 1, multiple multipaths can be calculated. All the multipath vectors can be added to the original signal separately and simultaneously in software. So a series of signals are generated as signal set

$$S_m = \{S(H_{m1}), S(H_{m2}), ..., S(H_{ml}), ...\}$$

Among the signal set, there is an optimal signal which can maximize the sensing performance. We select the optimal signal based on applications, which will be discussed in next section in detail.

### 3.3 Applying the proposed method to fine-grained activity sensing

To verify the effectiveness of the proposed approach in Section 3.2, we apply it to three fine-grained sensing applications: (1) respiration detection; (2) finger gesture recognition and (3) chin movement tracking when speaking. For different applications, we employ different optimal signal selection strategy and post-processing approaches. Before these operations, we adopt the Savitzky-Golay filter [22] to smooth the received raw noisy signal. Then we separately process the filtered signal and select the optimal multipath signal depending on application type.

**Respiration detection.** To detect human respiration rate, we utilize a band pass filter to retain the signal frequency component in 10-37 beats per minute (bpm) [16]. We extract the respiration rate using Fast Fourier Transform (FFT) [6]. The dominant frequency corresponds to the respiration rate of the target. To achieve best sensing performance, we select the optimal signal whose peak value in frequency domain is maximum to detect target's respiration rate.

**Finger gesture recognition.** To recognize various finger gestures, we design a selection algorithm based on the observation that the large amplitude variation is better than the small one for the same subtle movement. We obtain the difference between the maximum amplitude value and the minimum amplitude value of the signal in a sliding window (i.e., 1s in our implementation). Then we choose the optimal signal with the largest difference to recognize the finger gestures. Note that, there is a pause between the successive gestures, and the difference between the maximum amplitude value and the minimum amplitude value within this pause period is very small. We can thus employ this difference to detect pauses and segment the signal for each gesture. A dynamic threshold (i.e., 0.15 times of the difference in a window size) is set to detect the pause. At last, we employ a modified 9-layer neural network LeNet 5 [11] to recognize the gestures.

**Chin movement tracking when speaking.** To achieve the best performance for chin movement tracking, we apply the selection and segmentation algorithm mentioned in finger gesture recognition. Due to the single signal pattern of chin movement, we can choose the optimal signal with the largest variance to segment. After segmenting, each fragment corresponds to a word. Then an advanced peak finding algorithm [16] which can remove fake peaks is employed to count the syllable number for each word, which further constitutes sentences.

## 4 VERIFY THE AFFECTING FACTORS WITH BENCHMARK EXPERIMENTS

In this section, we carry out benchmark experiments in an anechoic chamber to verify the proposed theory and the effects of the three affecting factors described in Section 3.1.

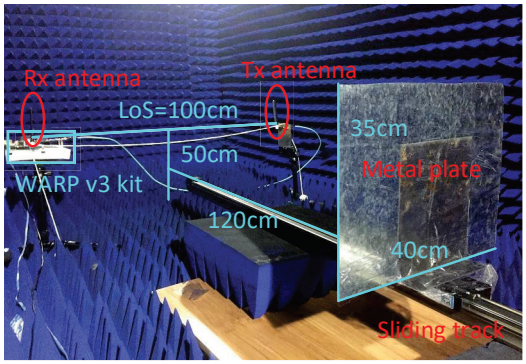


**Figure 10: Experimental deployment in an anechoic chamber**

**Experimental setting**: To minimize the amount of multipath interference, our experiments are carried out in an anechoic chamber as shown in Figure 10. The Rice WARP v3 platform [1, 2] is employed as the transceivers. The WARPLab implementation [3] is used to collect Wi-Fi packet samples. We configure one programmable RF interface of WARP as the transmitter and one as the receiver. Each RF interface is equipped with one omni-directional

antenna. A Dell laptop (Precision 5520) with Xeon CPU and 16G RAM is connected to WARP via an Ethernet cable to collect packet samples and process the data. The wireless signal is transmitted in the 5.24GHz frequency band with a 40MHz channel bandwidth. The antennas are placed perpendicular to the ground surface with a height of 50cm as shown in Figure 10. The LoS distance between the transceivers is set as 100cm. We employ a metal plate with a size of $35cm \times 40cm$ as the target. And the metal plate moves along the perpendicular bisector of the transceivers with the help of a sliding track which is controlled by Raspberry Pi 3 Model B [4].

**Experiment 1: Verify the basic model**. We move the metal plate along the perpendicular bisector of the transceivers from[3] 89cm to 79cm at a speed of $1cm/s$ with the help of a sliding track. According to the vector representation model described in Section 3, the dynamic vector rotates with the static vector. When the dynamic path length changes $\lambda$, the dynamic vector rotates 360°. The results are shown in Figure 11 and we can see that the dynamic vector generates close to perfect circles, demonstrating the correctness of the model. In Figure 11, the black dot is the origin of the coordinates. We can see that dynamic vector rotates clockwise, and the rotation phase is exactly matching with the theoretical rotation phase 1080° (3 circles). Besides, the magnitude of dynamic vector remains approximately the same in a short movement distance, which satisfies the hypothesis we made in Section 3.1.

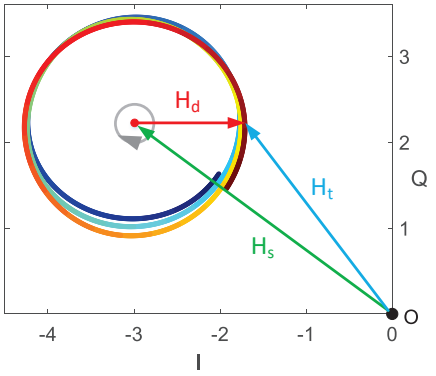


**Figure 11: Verify the model. The change in color of the curve describes the time series. From blue to red means varying from beginning to end.**

**Experiment 2: Verify the effect of the magnitude of the dynamic vector** ($|H_d|$). We move the metal plate along the perpendicular bisector of transceivers from 90cm to 50cm away from LoS at the speed of $1cm/s$. From Figure 12, we can see that the amplitude variation is around 2.5dB at distance 90cm and gradually increases to 4.5dB at distance 50cm. These results are consistent with the theoretical analysis: the further the metal plate is, the smaller the amplitude variation is. This is because the reflection signal attenuates with longer propagation distance [8].

**Experiment 3: Verify the effect of sensing capability phase** ($\Delta\theta_{sd}$). The metal plate repetitively moves along the sliding track

[3] 89cm and 79cm are measured from the metal plate to the LoS path of the transceiver pair.

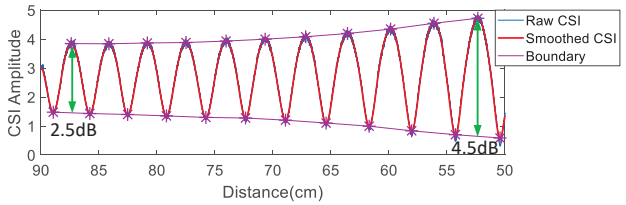


**Figure 12: Verify the effect of position**

at a small scale to mimic the fine-grained activity, e.g, human respiration. For each motion cycle, the metal plate moves forward $5mm$ and then moves backward $5mm$. We evaluate the sensing capability at 10 positions with adjacent positions spaced by 5mm. The first position is at 60cm from the LoS path. At each position, the metal plate performs 10 repetitive cycles of movements. Figure 13 shows the signal variation throughout the process. We observe that the sensing capability changes with the position of the metal plate. At the beginning, the metal plate is located at a bad position for sensing, at where the signal variation can not be identified. Then when the metal plate moves forward by just 5mm, we reach a good position with clearer and stronger signal variation. When the metal plate moves forward by another 5mm, the target is still at a good position. Finally the metal plate moves to a relatively bad position. The experimental results obtained during this process match the theoretical results in Figure 5 well. Note that, we can still observe clear fluctuation at a bad position for metal plate. However, for a human target, the signal induced is much weaker than the metal plate, which is easily merged by noise and can not be detected at bad positions.

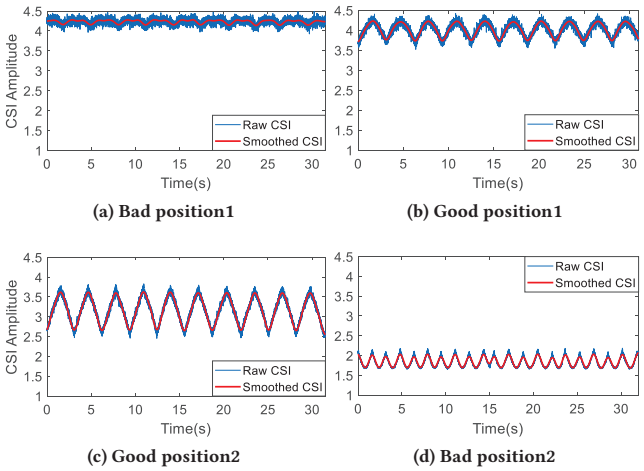


**Figure 13: Verify the effect of sensing capability phase**

**Experiment 4: Verify the effect of the phase change of the dynamic vector** ($\Delta\theta_{d12}$). We place the metal plate at 60cm from the LoS path. The same as in Experiment 3, we mimic the subtle movement of the fine-grained activities. For Case 1, the metal plate moves forward for $5mm$ and then backward for $5mm$. For Case 2, the metal plate moves forward and backward for $10mm$. We perform 10 repetitive motions for both Case 1 and Case 2. The amount of motion

displacement is linearly related to the phase difference $\Delta\theta_{d12}$. We compare the sensing capability of the two cases. From Figure 14, we can see that the signal amplitude variation (1.8dB) for Case 2 is clearly larger than that (0.7dB) of Case 1. This demonstrates that a larger movement displacement increases the sensing capability.

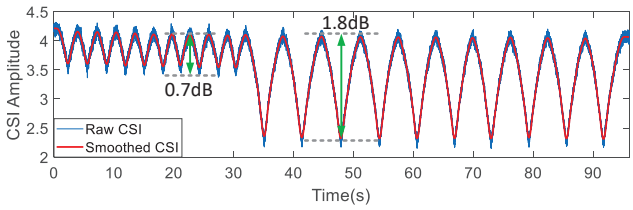


**Figure 14: Verify the effect of motion displacement**

So far, we have verified the factors affecting the sensing performance of fine-grained movements. We reveal the reason behind the unstable sensing performance and also show how to locate those "blind spots" with poor performance.

## 5 EVALUATION

We evaluate the performance of the proposed approach on three device-free fine-grained sensing applications: (1) respiration detection; (2) finger gesture recognition and (3) chin movement tracking when speaking.

### 5.1 Experimental setup

We implement our prototype system on WARP platform [1, 2] integrated with a Virtex-6 FPGA. We place the transmitter and receiver with a distance of 100cm between each other at the same height. The signal is transmitted in the 5.24GHz frequency band with a 40MHz channel bandwidth. For the three fine-grained sensing applications as shown in Figure 15, we adopt different methods to record the ground truths. The respiration rate is recorded by a fiber-based system (VitalPro 4374 Fiber Sensor Mat). The groundtruth of finger gesture recognition is recorded by a video camera. For chin movement tracking, we utilize a voice recorder to capture each spoken syllable.

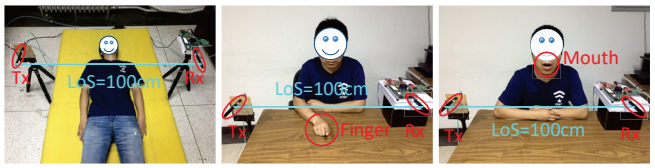


**(a) Respiration detection (b) Finger gesture recognition (c) Chin movement tracking**

**Figure 15: Real deployment using WARP platform for fine-grained activity sensing**

### 5.2 Leveraging multipath to change the effect of respiration detection

For respiration sensing, we recruit five participants and each of them is asked to lie on bed and breathe naturally. We record the respiration data for each participant. Figure 16a shows the smoothed signals for respiration sensing at a bad position. We observe that the original raw signal does not show periodic variations. By introducing different amounts of phases to the added multipath vector, Figure 16b-16d show the signal variations with 30°, 60° and 90° sensing capability phase shift, respectively. We can see that for a bad sensing position, the signal variation and accordingly the respiration sensing performance is significantly enhanced with carefully designed multipath, demonstrating the effectiveness of our proposed method.

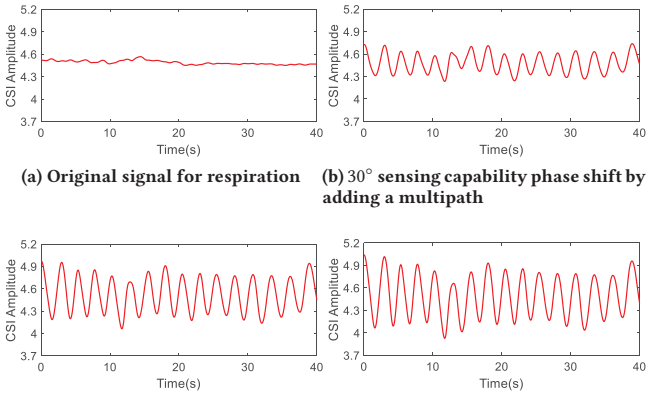


**(a) Original signal for respiration** **(b) 30° sensing capability phase shift by adding a multipath**

**(c) 60° sensing capability phase shift by adding a multipath** **(d) 90° sensing capability phase shift by adding a multipath**

**Figure 16: The effect of different multipaths in respiration sensing**

### 5.3 Achieving full coverage respiration detection

It is critical to remove the "blind spots" and achieve a full coverage for respiration sensing. We employ a heatmap of simulation to visualize the sensing capability information at each location. We generate the heatmap of respiration sensing at different locations in Figure 17a without our proposed method. We can see bad positions and good positions appear alternatively.

Inspired by building orthogonal static vector to achieve the complementation, we construct a multipath vector to shift the phase of static vector by $\pi/2$. Figure 17b demonstrates the results after introducing this multipath. We can clearly observe a reversed alternating pattern, the bad positions transform to good positions and vice versa. Combining these two heatmaps, the new sensing heatmap has no "blind spots" and good sensing performance can be achieved at all locations as shown in Figure 17c.

We further validate the full coverage respiration sensing performance in a real office environment as shown in Figure 15a. We deploy the WARP transceivers with a distance of 100cm between each other and the height is changed from 20cm to 100cm at a step size of 10cm. We ask each participant to lie on the bed and

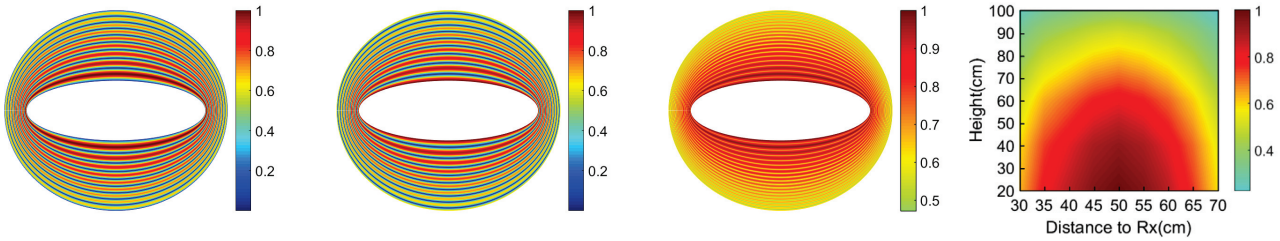


(a) Original simulated results (b) Orthogonal phase transform (c) Combination results (d) Real deployment results

**Figure 17: Sensing heatmap for respiration detection (Red color indicates good positions and blue color indicates bad positions)**

breathe naturally. The participant moves his position and the distance between the participant and the transmitter (Rx) is varied from 30cm to 70cm at a step size of 5cm. Note that the the sensing area is divided into grids with a size of $5cm \times 10cm$. From Figure 17d, we can see that the "blind spots" are removed with the proposed method and good respiration sensing performance is achieved at all the positions. For the five participants, we achieve an average respiration rate sensing accuracy of 98.8% across all the grids.

## 5.4 Enhancing finger gesture recognition

Contactless finger gesture recognition is an attractive human-computer interaction method. For example, finger gesture can be used to control home appliances such as TV and lights. In this work, we design eight finger gestures for control functions including return *console*, adjust *mode*, go *back*, *turn* on/off, *yes* to confirm, *no* to cancel, *up* to go to previous page or turn up volumes, *down* to go to next page or turn down volumes as shown in Figure 18. Taking memorability into consideration, the finger gestures mimic their original handwriting counterparts in one-dimension, which only needs to move finger up and down (as shown in Figure 18). For instance, the finger gesture for "m (mode)" is "up-down-up-down". The gesture design also employs moving distance of the finger (i.e. around 2cm for short and around 4cm for long) for differentiation.

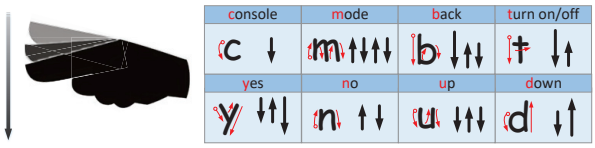


**Figure 18: Finger gestures design**

Now we show the capability of multipath to enhance the performance of finger gesture recognition. The experimental deployment is shown in Figure 15b. We recruit five participants to perform finger gestures. We take gesture *yes* and gesture *up* as examples. Figure 19a and Figure 19b depict the sensing signal at a bad position for gesture *yes* and gesture *up*, respectively. After introducing a multipath with 60° and 270° phase shift respectively, we observe obvious and unique signal variations appear in Figure 19c and Figure 19d. We can employ the induced unique variation pattern to identify each gesture. Figure 20 shows the accuracy performance

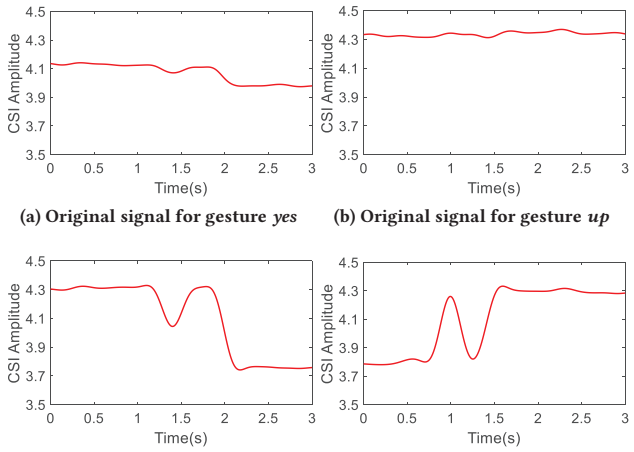


(a) Original signal for gesture *yes* (b) Original signal for gesture *up*

(c) Transformed signal for *yes* (d) Transformed signal for *up*

**Figure 19: The changing effect of finger gesture recognition.**

of finger gesture recognition without and with proper multipath. The overall recognition accuracy is increased from 33% to 81% on average.

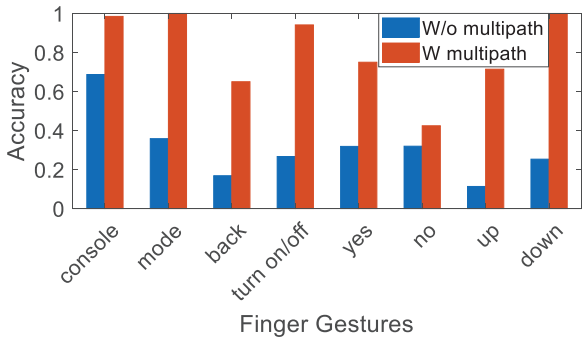


**Figure 20: Accuracy for finger gesture recognition.**

## 5.5 Enhancing the chin movement tracking

Now we carry out experiments to evaluate how the multipath improves the performance of chin movement tracking when speaking.

The two transceivers are placed with a distance of 100cm at the same height, shown in Figure 15c. The participants are asked to read two sentences "How are you? I am fine" and "Hello, world". All the words in the first sentences are monosyllabic while the second sentence contains two disyllable words. The participant's chin exhibits subtle movement during the process of pronouncing each syllable. The speaking process is recorded by a voice recorder as ground truth. Figure 21a and Figure 21b show the original sensing signal when reading these two short sentences. We are not able to see obvious signal variations corresponding to the chin movement. Then we introduce a multipath with 90° phase shift to enhance the sensing effect. Figure 21c shows the enhanced result when reading the first sentence and we can observe six clear valleys corresponding to the six syllables, which exactly match the ground-truth audio signal. For the second sentence in Figure 21d, we can also accurately obtain the syllables of each word and each word contains two valleys.

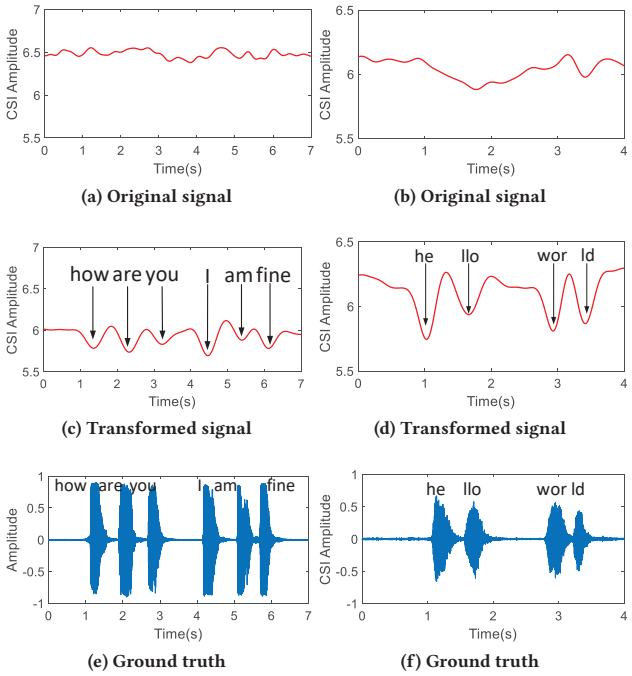


(a) Original signal (b) Original signal

(c) Transformed signal (d) Transformed signal

(e) Ground truth (f) Ground truth

**Figure 21: The changing effect of chin movement tracking when speaking.**

To show the overall performance, we recruit five participants to read multiple sentences. Each sentence contains 2-6 words. The sentences contain "I do", "How are you", "How do you do", "How can I help you", "What can I do for you", etc. The syllables include [e],[i],[u],[s], [l],[m],[h],[k],[w], etc. We evaluate the performance of counting the number of syllables in a spoken sentence. Figure 22 shows the confusion matrix for syllable counting accuracy. Without any learning algorithm, the average counting accuracy achieved is 92.8%. There is no significant difference in counting accuracy when the number of syllables increases.

| | | | | | |
|---|---|---|---|---|---|
| 2 | 1.0 | 0.0 | 0.0 | 0.0 | 0.0 |
| 3 | 0.06 | 0.91 | 0.03 | 0.0 | 0.0 |
| 4 | 0.0 | 0.03 | 0.90 | 0.07 | 0.0 |
| 5 | 0.0 | 0.0 | 0.06 | 0.91 | 0.03 |
| 6 | 0.0 | 0.0 | 0.03 | 0.05 | 0.92 |
| | 2 | 3 | 4 | 5 | 6 |

Number of syllables

**Figure 22: Accuracy for chin movement tracking when speaking.**

## 6 DISCUSSION

**The effect of secondary reflections.** Besides the direct reflection from the human target, there exist secondary reflections which bounce off the human target first and then bounce off other objects in the environment before reaching the receiver. In general, the secondary reflections are much weaker which can be ignored [8]. In some special scenarios when the target performs activities near to the wall, the secondary reflections can be relatively strong. We design an experiment to detect the target's respiration when the target is near to a large metal plate which creates strong secondary reflections. The experimental results show that even in this scenario with strong secondary refections, our method is robust and the sensing performance is hardly affected.

**The strength of the dynamic and static vectors.** Based on the relative signal strength between the dynamic and static vectors, we have three cases: *Case 1*: the dynamic vector is smaller than the static vector; *Case 2*: the dynamic vector is comparable with the static vector and *Case 3*: the dynamic vector is larger than the static vector. For fine-grained activity sensing, the two transceivers are placed close to each other with a direct LoS path. In the deployment with clear LoS path, the dynamic vector is much smaller than the static vector (Case 1). The proposed method works well in this case. If the LoS path is totally blocked or attenuated to be smaller than the dynamic vector, we fall into Case 3 and our method has difficulty to achieve the required amount of phase shift for performance enhancement. Thus it is suggested to have clear LoS path for the proposed method to work properly.

**Interference from surrounding people.** People walking around bring in interference for sensing. However, the interference due to surrounding people's movements is quite limited as the target is still closer to the transceiver pair. Thus, the interference can be filtered out with the Savitzky-Golay filter described in Section 3.3. On the other hand, dealing with interference from the target's other body parts is more challenging which remains an important future research topic for us.

**Work with commodity Wi-Fi card.** Our current implementation is based on WARP software-defined radio platform. It is challenging to have our system implemented on commodity Wi-Fi chipsets due to the changing Carrier Frequency Offset (CFO) and accordingly random phase readings for each packet. In the future, we plan to employ phase difference between adjacent antennas on the same Wi-Fi hardware to address this problem.

**Multi-target sensing.** It is challenging to passively sense multiple targets as the reflected signals from multiple targets are mixed together. New theory needs to be developed and this remains one important direction of our future research.

## 7 RELATED WORK

Contact-free human sensing using wireless technologies has drawn a lot of attentions from both academia and industry in recent years. Compared with computer vision-based approaches [18, 20], RF-based approaches can work without requiring a good lighting condition. A large variety of applications have been explored via wireless sensing, ranging from coarse-grained indoor localization [5, 14, 30, 32, 39], trajectory tracking [15, 21, 25, 35, 36], activity recognition [31] to fine-grained keystroke identification [7, 13], hand gesture recognition [12, 19, 23, 27], vital sign monitoring [6, 9, 16, 17, 29, 42–44], and speaking tracking [28]. However, most of these work employ pattern-based approaches that heavily rely on signal patterns and machine learning techniques, which cannot explain the reason why signal patterns vary at different locations, let alone improve the system performance via a controlled method.

Compared with pattern-based approaches, model-based approaches are studied to build the relationship between the received signal and human activities [37]. Wang et. al. [34] proposed the CSI-speed model which quantitatively establishes the relationship between the CSI value dynamics and human movement speeds to monitor and recognize activities. The model has been applied in coarse-grained activity recognition such as fall detection [34] and gait analysis [33]. Wu et. al. [38] and Wang et. al. [29] propose to apply the Fresnel Zone model for both coarse-grained and fine-grained human activity recognition. In particular, Wang et. al. [29] reveal that human respiration cannot be sensed at all locations with Wi-Fi signals and there are "blind spots" in the sensing area. In order to mitigate the "blind spots" problem, they proposed to use a linear motor to change the location of the Wi-Fi transceivers which is not realistic in real-life.

To cope with the multipath issue in wireless sensing, UWB [24, 26] technology with wide bandwidth (over 500MHz) is employed to reduce the influence of multipath, whereas the bandwidth of Wi-Fi signal is usually no more than 40MHz. For Wi-Fi based sensing, some systems [28, 30, 32, 40] try to eliminate or avoid the effect of multipath. For example, LiFS [32] removes the subcarriers which are greatly affected by multipath, MFDL [30] calibrates the phase difference to reduce the influence of multipath. WiHear [28] leverages MIMO beamforming to reduce irrelevant multipath effects introduced by omni-directional antennas, while WiWho [40] removes the distant multipath by converting CFR to CIR. As far as we know, there is no work trying to employ the phase difference between the dynamic multipath vector and static multipath vector to improve the sensing performance. We address the unstable sensing performance and "blind spots" issue by adding a carefully designed man-made "virtual" static multipath.

## 8 CONCLUSION

In this paper, we analyze and identify the major factors that affect the performance of fine-grained human activity sensing. By analyzing the relationship between the static and dynamic signals, we discover that the phase difference between the static and dynamic vector determines the sensing performance at each location. We thus propose to add a carefully designed "virtual" multipath to boost the sensing capability of the fine-grained human activity to its maximum at each location. We apply the proposed method on three fine-grained sensing applications and comprehensive experimental results demonstrate the effectiveness of the proposed method. We envision the proposed method can also be applied to improve the sensing performance of other wireless technologies such as RFID or sound.

## ACKNOWLEDGMENTS

This work is supported by the National Natural Science Foundation of China (Grant No. 61572048), the National Key Research and Development Plan (Grant No. 2016YFB1001200), and the Young Scientists Fund of the National Natural Science Foundation of China (Grant No. 61802373).

## REFERENCES

[1] 2017. Mango Communications. http://mangocomm.com. Online, accessed 1-October-2017.
[2] 2017. WARP Project. https://warpproject.org. Online, accessed 1-October-2017.
[3] 2017. WARPLab 7. https://warpproject.org/trac/wiki/WARPLab. Online, accessed 1-October-2017.
[4] 2018. Raspberry Pi 3 Model B. https://www.raspberrypi.org/products/raspberry-pi-3-model-b/. Online, accessed 21-June-2018.
[5] Fadel Adib, Zachary Kabelac, and Dina Katabi. 2015. Multi-Person Localization via RF Body Reflections.. In *NSDI*. 279–292.
[6] Fadel Adib, Hongzi Mao, Zachary Kabelac, Dina Katabi, and Robert C Miller. 2015. Smart homes that monitor breathing and heart rate. In *Proceedings of the 33rd annual ACM conference on human factors in computing systems*. ACM, 837–846.
[7] Kamran Ali, Alex X Liu, Wei Wang, and Muhammad Shahzad. 2017. Recognizing keystrokes using WiFi devices. *IEEE Journal on Selected Areas in Communications* 35, 5 (2017), 1175–1190.
[8] Yibo Chen and Rong Luo. 2007. Design and implementation of a wifi-based local locating system. In *Portable Information Devices, 2007. PORTABLE07. IEEE International Conference on*. IEEE, 1–5.
[9] Chen-Yu Hsu, Aayush Ahuja, Shichao Yue, Rumen Hristov, Zachary Kabelac, and Dina Katabi. 2017. Zero-Effort In-Home Sleep and Insomnia Monitoring using Radio Signals. *Proceedings of the ACM on Interactive, Mobile, Wearable and Ubiquitous Technologies* 1, 3 (2017), 59.
[10] Chen-Yu Hsu, Yuchen Liu, Zachary Kabelac, Rumen Hristov, Dina Katabi, and Christine Liu. 2017. Extracting Gait Velocity and Stride Length from Surrounding Radio Signals. In *Proceedings of the 2017 CHI Conference on Human Factors in Computing Systems*. ACM, 2116–2126.
[11] Yann LeCun, LD Jackel, Leon Bottou, A Brunot, Corinna Cortes, JS Denker, Harris Drucker, I Guyon, UA Muller, Eduard Sackinger, et al. 1995. Comparison of learning algorithms for handwritten digit recognition. In *International conference on artificial neural networks*, Vol. 60. Perth, Australia, 53–60.
[12] Hong Li, Wei Yang, Jianxin Wang, Yang Xu, and Liusheng Huang. 2016. WiFinger: talk to your smart devices with finger-grained gesture. In *Proceedings of the 2016 ACM International Joint Conference on Pervasive and Ubiquitous Computing*. ACM, 250–261.
[13] Mengyuan Li, Yan Meng, Junyi Liu, Haojin Zhu, Xiaohui Liang, Yao Liu, and Na Ruan. 2016. When CSI meets public WiFi: Inferring your mobile phone password via WiFi signals. In *Proceedings of the 2016 ACM SIGSAC Conference on Computer and Communications Security*. ACM, 1068–1079.
[14] Xiang Li, Shengjie Li, Daqing Zhang, Jie Xiong, Yasha Wang, and Hong Mei. 2016. Dynamic-music: accurate device-free indoor localization. In *Proceedings of the 2016 ACM International Joint Conference on Pervasive and Ubiquitous Computing*. ACM, 196–207.
[15] Xiang Li, Daqing Zhang, Qin Lv, Jie Xiong, Shengjie Li, Yue Zhang, and Hong Mei. 2017. IndoTrack: Device-Free Indoor Human Tracking with Commodity Wi-Fi. *Proceedings of the ACM on Interactive, Mobile, Wearable and Ubiquitous*

*Technologies* 1, 3 (2017), 72.
[16] Jian Liu, Yan Wang, Yingying Chen, Jie Yang, Xu Chen, and Jerry Cheng. 2015. Tracking vital signs during sleep leveraging off-the-shelf wifi. In *Proceedings of the 16th ACM International Symposium on Mobile Ad Hoc Networking and Computing*. ACM, 267–276.
[17] Xuefeng Liu, Jiannong Cao, Shaojie Tang, and Jiaqi Wen. 2014. Wi-Sleep: Contactless sleep monitoring via WiFi signals. In *Real-Time Systems Symposium (RTSS), 2014 IEEE*. IEEE, 346–355.
[18] Huadong Ma, Chengbin Zeng, and Charles X Ling. 2012. A reliable people counting system via multiple cameras. *ACM Transactions on Intelligent Systems and Technology (TIST)* 3, 2 (2012), 31.
[19] Pedro Melgarejo, Xinyu Zhang, Parameswaran Ramanathan, and David Chu. 2014. Leveraging directional antenna capabilities for fine-grained gesture recognition. In *Proceedings of the 2014 ACM International Joint Conference on Pervasive and Ubiquitous Computing*. ACM, 541–551.
[20] Jochen Penne, Christian Schaller, Joachim Hornegger, and Torsten Kuwert. 2008. Robust real-time 3D respiratory motion detection using time-of-flight cameras. *International Journal of Computer Assisted Radiology and Surgery* 3, 5 (2008), 427–431.
[21] Kun Qian, Chenshu Wu, Zimu Zhou, Yue Zheng, Zheng Yang, and Yunhao Liu. 2017. Inferring motion direction using commodity wi-fi for interactive exergames. In *Proceedings of the 2017 CHI Conference on Human Factors in Computing Systems*. ACM, 1961–1972.
[22] Ronald W Schafer. 2011. What is a Savitzky-Golay filter?[lecture notes]. *IEEE Signal Processing Magazine* 4 (2011), 111 117.
[23] Longfei Shangguan, Zimu Zhou, and Kyle Jamieson. 2017. Enabling gesture-based interactions with objects. In *Proceedings of the 15th Annual International Conference on Mobile Systems, Applications, and Services*. ACM, 239–251.
[24] Liyuan Song, Hongliang Zou, and Tingting Zhang. 2015. A low complexity asynchronous UWB TDOA localization method. *International Journal of Distributed Sensor Networks* 11, 10 (2015), 675490.
[25] Li Sun, Souvik Sen, Dimitrios Koutsonikolas, and Kyu-Han Kim. 2015. Widraw: Enabling hands-free drawing in the air on commodity wifi devices. In *Proceedings of the 21st Annual International Conference on Mobile Computing and Networking*. ACM, 77–89.
[26] Swaroop Venkatesh, Christopher R Anderson, Natalia V Rivera, and R Michael Buehrer. 2005. Implementation and analysis of respiration-rate estimation using impulse-based UWB. In *Military Communications Conference, 2005. MILCOM 2005. IEEE*. IEEE, 3314–3320.
[27] Aditya Virmani and Muhammad Shahzad. 2017. Position and Orientation Agnostic Gesture Recognition Using WiFi. In *Proceedings of the 15th Annual International Conference on Mobile Systems, Applications, and Services*. ACM, 252–264.
[28] Guanhua Wang, Yongpan Zou, Zimu Zhou, Kaishun Wu, and Lionel M Ni. 2016. We can hear you with wi-fi! *IEEE Transactions on Mobile Computing* 15, 11 (2016), 2907–2920.
[29] Hao Wang, Daqing Zhang, Junyi Ma, Yasha Wang, Yuxiang Wang, Dan Wu, Tao Gu, and Bing Xie. 2016. Human respiration detection with commodity wifi devices: do user location and body orientation matter?. In *Proceedings of the 2016 ACM International Joint Conference on Pervasive and Ubiquitous Computing*. ACM, 25–36.
[30] Hao Wang, Daqing Zhang, Kai Niu, Qin Lv, Yuanhuai Liu, Dan Wu, Ruiyang Gao, and Bing Xie. 2017. MFDL: A Multicarrier Fresnel Penetration Model based Device-Free Localization System leveraging Commodity Wi-Fi Cards. *arXiv preprint arXiv:1707.07514* (2017).
[31] Hao Wang, Daqing Zhang, Yasha Wang, Junyi Ma, Yuxiang Wang, and Shengjie Li. 2017. RT-Fall: A real-time and contactless fall detection system with commodity WiFi devices. *IEEE Transactions on Mobile Computing* 16, 2 (2017), 511–526.
[32] Ju Wang, Hongbo Jiang, Jie Xiong, Kyle Jamieson, Xiaojiang Chen, Dingyi Fang, and Binbin Xie. 2016. LiFS: low human-effort, device-free localization with fine-grained subcarrier information. In *Proceedings of the 22nd Annual International Conference on Mobile Computing and Networking*. ACM, 243–256.
[33] Wei Wang, Alex X Liu, and Muhammad Shahzad. 2016. Gait recognition using wifi signals. In *Proceedings of the 2016 ACM International Joint Conference on Pervasive and Ubiquitous Computing*. ACM, 363–373.
[34] Wei Wang, Alex X Liu, Muhammad Shahzad, Kang Ling, and Sanglu Lu. 2015. Understanding and modeling of wifi signal based human activity recognition. In *Proceedings of the 21st Annual International Conference on Mobile Computing and Networking*. ACM, 65–76.
[35] Yan Wang, Jian Liu, Yingying Chen, Marco Gruteser, Jie Yang, and Hongbo Liu. 2014. E-eyes: device-free location-oriented activity identification using fine-grained wifi signatures. In *Proceedings of the 20th annual international conference on Mobile computing and networking*. ACM, 617–628.
[36] Teng Wei and Xinyu Zhang. 2015. mtrack: High-precision passive tracking using millimeter wave radios. In *Proceedings of the 21st Annual International Conference on Mobile Computing and Networking*. ACM, 117–129.
[37] Dan Wu, Daqing Zhang, Chenren Xu, Hao Wang, and Xiang Li. 2017. Device-Free WiFi Human Sensing: From Pattern-Based to Model-Based Approaches. *IEEE Communications Magazine* 55, 10 (2017), 91–97.
[38] Dan Wu, Daqing Zhang, Chenren Xu, Yasha Wang, and Hao Wang. 2016. WiDir: walking direction estimation using wireless signals. In *Proceedings of the 2016 ACM International Joint Conference on Pervasive and Ubiquitous Computing*. ACM, 351–362.
[39] Jie Xiong, Karthikeyan Sundaresan, and Kyle Jamieson. 2015. Tonetrack: Leveraging frequency-agile radios for time-based indoor wireless localization. In *Proceedings of the 21st Annual International Conference on Mobile Computing and Networking*. ACM, 537–549.
[40] Yunze Zeng, Parth H Pathak, and Prasant Mohapatra. 2016. WiWho: wifi-based person identification in smart spaces. In *Proceedings of the 15th International Conference on Information Processing in Sensor Networks*. IEEE Press, 4.
[41] Daqing Zhang, Hao Wang, and Dan Wu. 2017. Toward centimeter-scale human activity sensing with Wi-Fi signals. *Computer* 50, 1 (2017), 48–57.
[42] Fusang Zhang, Daqing Zhang, Jie Xiong, Hao Wang, Kai Niu, Beihong Jin, and Yuxiang Wang. 2018. From Fresnel Diffraction Model to Fine-grained Human Respiration Sensing with Commodity Wi-Fi Devices. *Proceedings of the ACM on Interactive, Mobile, Wearable and Ubiquitous Technologies* 1, 53 (2018).
[43] Mingmin Zhao, Fadel Adib, and Dina Katabi. 2016. Emotion recognition using wireless signals. In *Proceedings of the 22nd Annual International Conference on Mobile Computing and Networking*. ACM, 95–108.
[44] Mingmin Zhao, Shichao Yue, Dina Katabi, Tommi S Jaakkola, and Matt T Bianchi. 2017. Learning sleep stages from radio signals: A conditional adversarial architecture. In *International Conference on Machine Learning*. 4100–4109.